# Cycle-Resolved HWA Measurements with Single- and Dual-Sensor Probes in an Open-Chamber Automotive Engine

A.E.Catania, C.Dongiovanni, A.Mittica, G.Molina and E.Spessa

*Dipartimento di Energetica-Politecnico di Torino*
*Corso Duca degli Abruzzi, 24-10129 Torino*
*Italy*

## ABSTRACT

A sophisticated HWA technique has been enhanced by applying specifically oriented single and double sensor-wires to analyze the air mean-flow and turbulence properties in the cylinder of a motored automotive engine with a re-entrant in--piston bowl and one helicoidal intake duct.

Air-velocity measurements were taken along the injector axis at several distances from the cylinder head and engine speeds, in a range from 600 rpm to 3000 rpm. The three components of the mean motion were resolved along the axial, radial and tangential directions, respectively, in the cylinder reference frame. Shielded probes were used to determine the flow direction, whenever necessary, so as to remove any problems of directional ambiguity. The mean velocities obtained with single- and dual-sensor probes at the same locations and operating conditions were compared in order to assess the lack of reciprocal wire interference for these latter. The dependence of turbulence quantities on the measurement point and engine speed was preliminarily examined in addition to the direct- and reverse-squish effects on the time-frequency turbulence structure.

## INTRODUCTION

The increasing needs for higher-efficiency and lower pollutant-emission automotive engines to meet the ever more stringent regulations pose heavy demands on the effective utilization of the turbulent flow processes and on their control in the combustion system of recent engine design, such as DI diesel and stratified-charge engines. As is well known [1-4](*), the engine fluid-dynamics plays a major role in controlling the pollutant emission sources which are intimately coupled with the primary combustion process, while preserving the combustion quality in lean-mixture or recycled-exhaust engines. Therefore, the application of more sophisticated flow diagnostic techniques to these engines is fundamental for their performance improvement.

A new test bench was equipped and set up in [1] to investigate the effects of a re-entrant combustion bowl and one helicoidal intake duct on the in-cylinder fluid-dynamics of a production engine, with particular reference to the turbulence properties. To that end, an advanced HWA (hot-wire anemometric) technique has been improved by a more accurate gas temperature evaluation and by the development of probes with specifically oriented single and multiple wires.

For the first time were dual-sensor probes applied to in--cylinder air velocity measurements. Their use was substantiated through the comparison between the mean velocities measured by each sensing element of the probe and those obtained from single-sensor probes. The three components of the air mean flow were resolved with the support of shielded probes to determine the flow direction. An insight was also given into the production mechanisms of turbulence and its time-frequency structure at the end of the compression stroke along with the dependence of turbulence intensity and mean--flow cyclic fluctuations on the distance from the cylinder head and engine speed in a range from 600 rpm to 3000 rpm.

## IN-CYLINDER VELOCITY MEASUREMENTS

### Experimental System

The test engine (Fig.1) is a four-stroke, open-chamber single-cylinder with two valves, derived from a high compression-ratio production engine at the Fiat Research

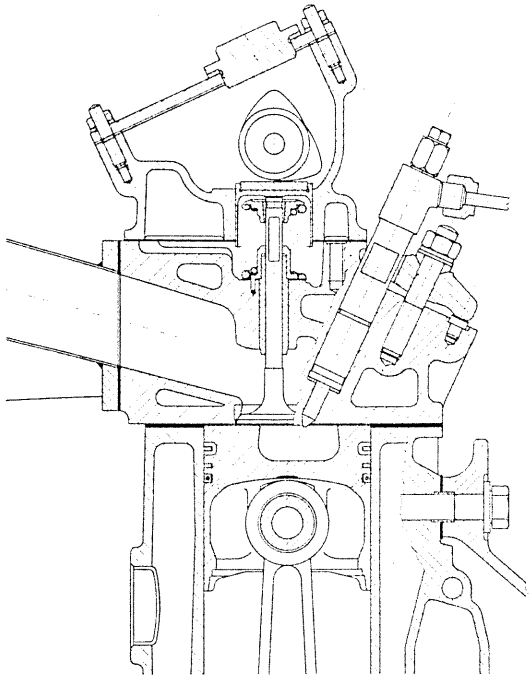

Fig. 1 - Test engine.

(*) Numbers in square brackets designate references at the end of paper.

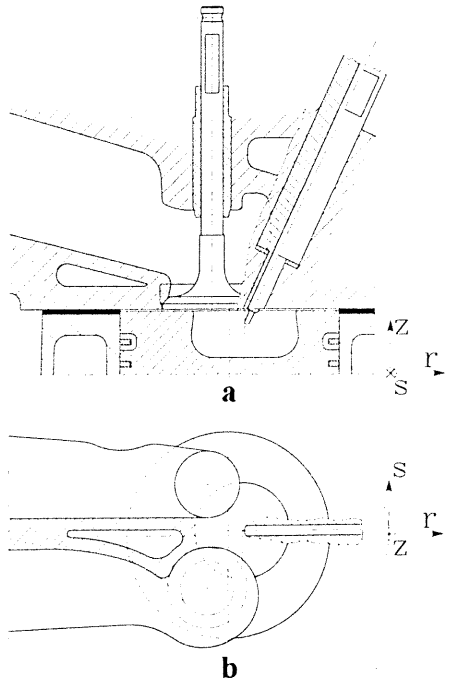


Fig. 2 - Schematic of the engine with probe setup.

Center. It has a high-squish in-piston bowl of the re-entrant type (Fig. 2a) and one helicoidal intake duct, inducing a counterclockwise swirling flow (Fig. 2b). The main engine specifications are: bore 79.5 mm; stroke 86 mm; compression ratio 18; inlet valve (i.v.) maximum lift 8.1 mm; i.v. opens 5 deg BTDC; i.v. closes 55 deg ABDC; exhaust valve (e.v.) opens 55 deg BBDC; e.v. closes 5 deg ATDC; speed range 500-3500 rpm. The single cylinder was motored by an electrical motor through a speed regulator of the belt type.

The in-cylinder air velocities were measured with the previously developed HWA technique [1], using constant--temperature units. Comments on the advantages and drawbacks of HWA versus LDV are reported in [2].

A schematic of the engine with the anemometric probe setup is shown in Fig. 2. The probe was accommodated in the injector seat without any modification to the engine design (Fig. 2a). The probe axis was coincident with the injector one and made a 25 deg (± 0.5 percent) angle with the cylinder axis. A specifically designed and built micrometric device allowed the probe displacement along its axis with an accuracy of ±0.05 mm.

Since the anemometric output depends not only on the gas velocity, but also on air temperature and pressure, as well as on the wire prong temperature, it was also necessary to measure these quantities. For pressure measurements, a piezoelectric transducer was accommodated in the glow-plug seat. The same anemometric probe was alternatively used as a thermometric one for gas temperature measurements. In this case the probe was made one arm of a wheatstone bridge supplied by a carrier-frequency power amplifier. The air velocity and temperature data were thus acquired at the same point, under the same operating conditions, though not at the same instant. In fact, the thermometric-wire traces showed a high cycle-to-cycle repeatability, being slightly affected by cyclic velocity fluctuations. The prong temperature at their tip, where the sensing wire is welded, was measured by means of a thermocouple, one of its leads being a prong.

In order to evaluate the velocity components, three types of single-wire probes were built, with the sensing element oriented along the radial, tangential and axial direction, respectively, in the cylinder reference frame. For the first time, dual-sensor probes were also applied to the in-cylinder mean-flow analysis. These were constructed with couples of mutually orthogonal wires oriented along two of the above mentioned directions. In the present work, only those with wires along the radial and tangential directions were used.

Data-Acquisition System

An automatic data-acquisition system with three 12 bit analog-to-digital (A/D) converters and a high-speed memory buffer was used [1]. This configuration allows the acquisition of up to 655360 samples from three different channels simultaneously. The maximum sample rate is 500 kHz when only one channel is employed and becomes 150 kHz per channel when data are acquired from three different sources. The acquisition process was governed by an external trigger signal, which was produced by a crank-shaft driven encoder. This is provided with 1800 angular divisions and generates an impulse every 0.2 crank-angle deg. An acquisition controller was directly interfaced to the system through a dedicated high transfer rate connection (180 kHz), for data processing in real time. The data-capture was managed by a specifically developed software based on a programming package which supports the system card functions [1].

In previous investigations on a different engine [3, 4], the in-cylinder flow was analyzed during the intake and compression strokes. In the present work the data acquisition

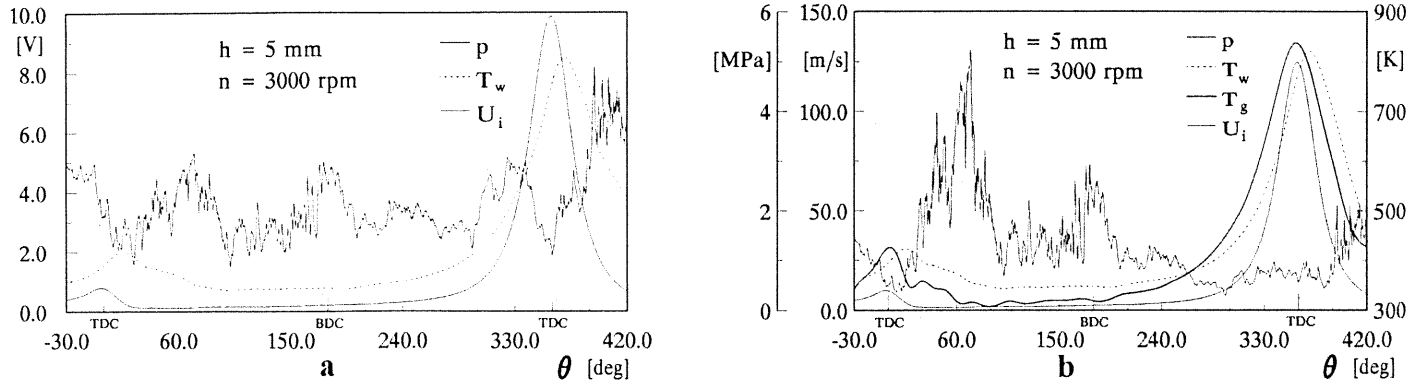


Fig.3 - Cycle-resolved piezometric, thermometric and anemometric data records (a) and related quantities (b) obtained by a single-sensor probe with axial wire.

interval was extended to 30 crank-angle deg before TDC where the inlet-valve opening occurred, and also to 60 deg after the end of the compression stroke, in order to investigate the squish flow produced by the combustion bowl at the beginning of the expansion stroke. In what follows, the start of the induction stroke at TDC will be taken as 0 crank--angle deg ($\theta = 0$ deg). Figure 3a gives an example of the piezometric ($p$), thermometric ($T_w$) and anemometric ($U_i$) traces versus crank angle ($\theta$), acquired in an engine cycle.

Experimental Data Processing

The cooling velocity $U_i$ was computed from the anemometer output signal as detailed in [1]. The procedure is based on the analytical solution of thermometric and anemometric wire heat-transfer equations and takes into account the gas property influence, the prong temperature effect and the thermometric sensor lag. Fig. 3b shows the distributions of pressure ($p$), wire ($T_w$) and gas ($T_g$) temperatures as well as of air velocity ($U_i$) versus crank angle, obtained from the data records of Fig. 3a.

At each measuring point the cooling velocities $U_R$, $U_T$ and $U_A$ are measured with the wires oriented along the radial (R), tangential (T) and axial (A) directions, respectively. The correlations between these velocities and the actual velocity components $V_r$, $V_s$ and $V_z$ in the radial (r), tangential, or swirl (s) and axial (z) directions are given by:

$$V_r^2 = \frac{-(1+\chi^2)U_R^2 + U_T^2 + U_A^2}{(1-\chi^2)(2+\chi^2)}$$

$$V_s^2 = \frac{-(1+\chi^2)U_T^2 + U_R^2 + U_A^2}{(1-\chi^2)(2+\chi^2)} \qquad (1)$$

$$V_z^2 = \frac{-(1+\chi^2)U_A^2 + U_T^2 + U_R^2}{(1-\chi^2)(2+\chi^2)}$$

$\chi$ is an empirical factor taking into account the cooling effect of the velocity component along the wire axis. A value of $\chi \approx 0.18$ was used [1].

Determination of Flow Direction

Special single-sensor probes with shielded wires (Fig. 4) were used to determine the flow direction, whenever necessary. Fig. 5 shows the ensemble average of anemometer signals obtained by means of a shielded probe (shield b of Fig. 4) with radial wire. The thick line in the figure was obtained with the wire facing the clockwise flow, while the thin one refers to the counterclockwise-flow facing wire. The difference between the two signals supports the distribution of the tangential velocity component in Fig. 10b, showing a positive (counterclockwise) $V_s$ during the intake stroke (as is

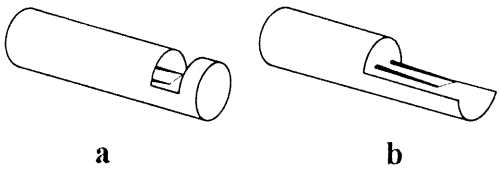

a b

Fig.4 - Types of shield used on hot-wire probes.

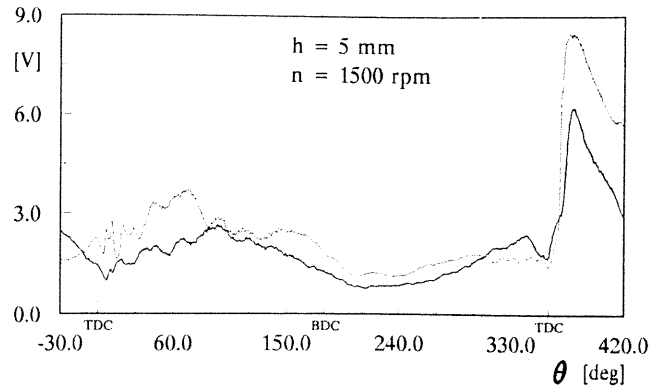


Fig.5 - Ensemble-averaged anemometric signals of shielded probes (Fig. 8b) with radial wire facing clockwise flow (thick line) and counterclockwise flow (thin line), respectively.

physically consistent with the duct geometry) and a reversal of the swirl component at the end of the compression stroke.

Experimental Uncertainties

The method used to compute air velocity from the anemometer output was validated in nonstationary as well as stationary conditions, at different gas pressures and temperatures [3, 4]. It is different from all of those semiempirical corrections considered in [5], as specified in [4]. Based on previous findings [3] and on the average deviations of repeated measurement sets, a maximum uncertainty of $\pm 10$ percent could be generally ascribed to the computed velocity, though it would be safer to assign an uncertainty interval of $\pm 12$ percent to the velocity during the reverse--squish phase at the beginning of the expansion stroke, owing to a lower flow-property repeatability at that stage.

The statistical uncertainty in autospectra estimates depends on the reciprocal square root of the number of data records [2] and could be considered as less then 12 percent in the presented results.

## CYCLE-RESOLVED APPROACH

The time-average filtering (TAF) procedure [4, 6] was used to determine the in-cycle nonstationary mean-velocity from each single data record. It is based on the interpolation of mean value estimates obtained by time-averaging the velocity in discrete crank-angle intervals throughout the engine cycle and is able to yield a cycle-resolved turbulent velocity fluctuation with a zero mean value, either as a time--averaged value in each cycle or, approximately, as an ensemble-averaged value over many cycles [6]. A spline operator was used for interpolation, though different types of interpolating functions were shown to yield no significantly different results [6].

## TURBULENCE PROPERTIES

Averaging Operators

The overscore or bar is used to indicate a time--averaging operation over a finite interval, that is a short--time-averaging operation. Therefore, $\bar{f}_i$ represents the time average of any variable $f_i(t)$ (or $f_i(\theta)$) in the interval $T$

centered on the instant $t_0$ (or in the crank-angle interval $\Theta$)

$$\bar{f}_i = \frac{1}{T}\int_{t_0-T/2}^{t_0+T/2} f_i(t)dt = \frac{1}{\Theta}\int_{\theta_0-\Theta/2}^{\theta_0+\Theta/2} f_i(\theta)d\theta \qquad (2)$$

The brackets $\langle\ \rangle$ denote an average taken over a large number of sample records, that is, an ensemble average. Therefore, $\langle f_i(t)\rangle$ represents the ensemble average of the variable $f_i(t)$ at the time $t$ over $N$ records (or cycles)

$$\langle f_i(t)\rangle = \frac{1}{N}\sum_{i=1}^{N} f_i(t) \qquad (3)$$

Turbulent Velocity Fluctuations

Any component of the instantaneous velocity in the cylinder of a reciprocating internal combustion engine can be split into a mean nonstationary part along its direction and a turbulent fluctuation about this mean, so that, with reference to the engine cycle $i$

$$U_i(t) = \tilde{U}_i(t) + u_i(t) = U(t) + \tilde{u}_i(t) + u_i(t) \qquad (4)$$

where: $\tilde{U}_i(t)$ is the cycle-resolved mean velocity, $u_i(t)$ the cycle-resolved velocity fluctuation about the mean, $U(t)$ the ensemble-averaged mean velocity and $\tilde{u}_i(t)$ the so called low-frequency cyclic fluctuation of the mean velocity [2].

In the conventional ensemble-averaging approach, equation (4) is replaced by

$$U_i(t) = U_E(t) + u_{i,E}(t) \qquad (5)$$

where the mean velocity, that is the ensemble-averaged velocity $U_E(t) = \langle U_i(t)\rangle$, is the same in each cycle; the turbulent fluctuation $u_{i,E}(t)$ about $U_E(t)$ will also be simply referred to as the instantaneous velocity fluctuation.

By ensemble-averaging all terms in equation (4) and using the symbol $\varepsilon(t)$ to designate the ensemble average of $u_i(t)$, one obtaines from equations (4) and (5)

$$u_{i,E}(t) = u_i(t) + \tilde{u}_i(t) - \varepsilon(t) \approx u_i(t) + \tilde{u}_i(t) \qquad (6)$$

The intensity of the instantaneous velocity fluctuation is

$$u'_E(t) = \sqrt{\langle u_{i,E}^2(t)\rangle} \qquad (7)$$

Within the TAF procedure, the ensemble-averaged turbulence intensity $u'$ and the rms fluctuation of the in-cycle mean velocity $U_{rms}$ in the interval $T$ are defined as

$$u' = \sqrt{\langle \overline{u_i^2} \rangle} \qquad \text{and} \qquad U_{rms} = \sqrt{\langle \overline{\tilde{u}_i^2} \rangle} \qquad (8)$$

The basic requirements to fit the averaging crank-angle interval $\Theta$ for selection were specified in [4, 6]. In the present work, a crank-angle $\Theta$ = 15 deg was chosen.

Time-Frequency Spectral Functions

The Eulerian time autocorrelation coefficient of the turbulent fluctuation $u_i(t)$ in the period $T$, centered on the instant $t_0$, can be defined as follows [2, 7, 8]

$$R_{uu}(T,t_0,\tau) = \frac{1}{u'^2}\left\langle \frac{1}{T-\tau}\int_{t_0-T/2+\tau/2}^{t_0+T/2-\tau/2} u_i(t-\tau/2)u_i(t+\tau/2)dt \right\rangle \qquad (9)$$

The separation-time variable $\tau$ in the correlation interval $T$ ranges from zero to $\tau_{max} = T/2$. The factor $u'^2$, normalizing the autocorrelation function to unity at $\tau = 0$, is the square of the turbulence intensity in $T$. The autocorrelation coefficient given by equation (9) (being an even function of $\tau$, independent of the instant $t$ in the period $T$) makes the standard approach for stationary flows [9, 10] suitable also for the spectral analysis of nonstationary turbulent fluctuations in sub-records into which the acquired data record was divided.

The normalized energy spectral density function of the turbulent fluctuation $u_i(t)$ in $T$, can be obtained from equation (9) as follows [2]

$$E_{uu}(T,t_0,f) = 4\int_0^{\tau_{max}} R_{uu}(T,t_0,\tau)w(\tau)\cos(2\pi f\tau)d\tau \qquad (10)$$

where $f$ is the frequency and $w(\tau)$ is a window function of the rectangular or Hamming type. In order to analyze the turbulence structure throughout the engine cycle, discrete correlation crank-angle intervals $\Phi$, each corresponding to the period $T$ in equation (9) or (10), were considered. These should be long enough to provide statistical validity of the results, but, at the same time, short enough to include a negligible effect of the turbulence time-dependence. Based on previous experiences [2, 8] a crank-angle $\Phi$ = 60 deg was used for turbulence spectral analysis.

Though equations (9) and (10) are written for the cycle-resolved turbulent fluctuation, similar expressions can be derived for any of the other fluctuation terms in equation (6), as shown in [2]. In what follows, the symbols $R_{u_E u_E}$ and $E_{u_E u_E}$ will be used to express the autocorrelation coefficient and the normalized spectral density function of the instantaneous velocity fluctuation, respectively.

## EXPERIMENTAL RESULTS AND DISCUSSION

Velocity measurements were carried out at three different locations along the injector axis; the locations were at levels ($h$) of 2 mm, 5 mm and 9 mm underneath the flat cylinder head, and at radial distances from the cylinder axis of 5.9 mm, 4.5 mm and 2.6 mm, respectively. A number from 100 to 500 anemometric data records were taken for each measurement set.

Figures 6 - 8 give examples of instantaneous velocity records versus crank angle, with related mean velocities and turbulent fluctuations determined either by conventional ensemble-averaging (Fig. 6) or using the TAF procedure (Figs. 7 and 8). The velocity traces of Figs. 6 and 7 were obtained in the same engine cycle with the radial (Figs. 6a and 7a) and the tangential wire (Figs. 6b and 7b) of a dual-sensor probe, at a distance $h$ = 2 mm from the cylinder head and at an engine speed $n$ = 600 rpm; the results of Fig. 8 were obtained, at $h$ = 5 mm and $n$ = 3000 rpm, by a single-sensor probe with the wire oriented along the axial (Fig. 8a) and the tangential (Fig. 8b) directions. In the instantaneous

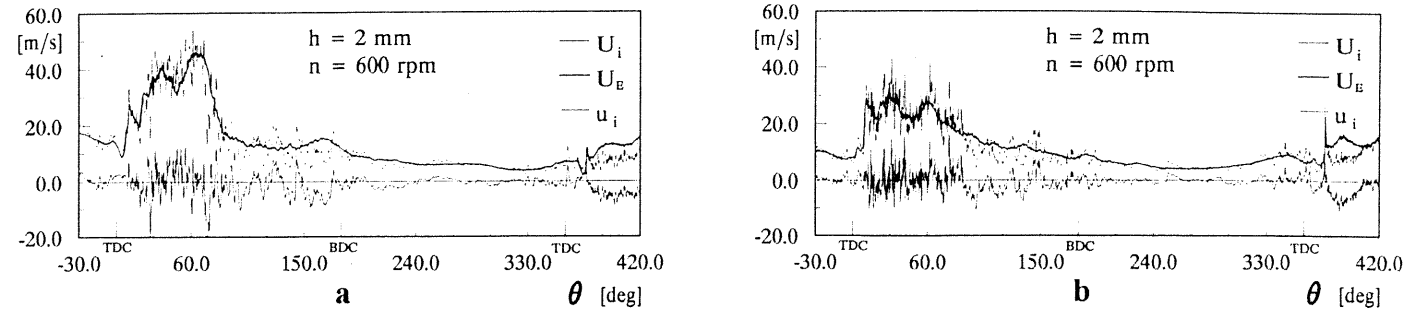


Fig. 6 - Instantaneous velocity, mean velocity and turbulent fluctuation obtained by the radial (a) and tangential (b) wires of a dual-sensor probe in the same engine cycle (ensemble-averaging procedure).

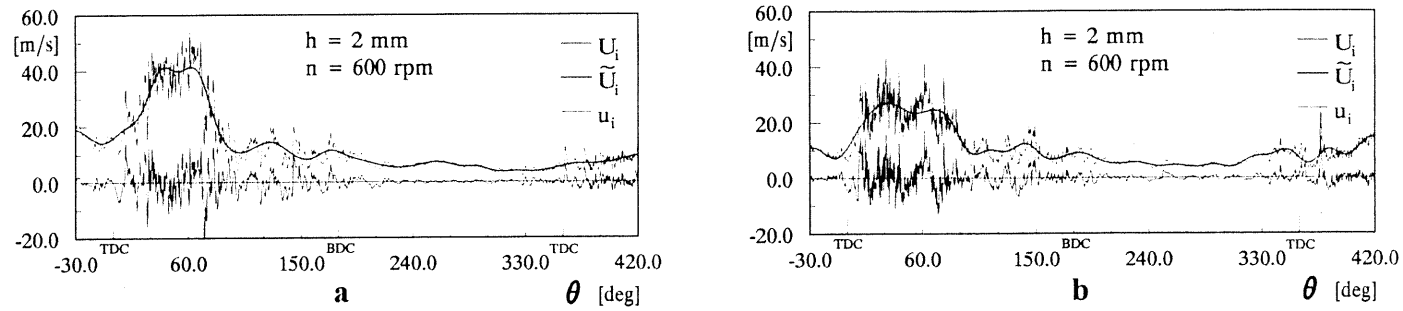


Fig. 7 - Instantaneous velocity, mean velocity and turbulent fluctuation obtained by the radial (a) and tangential (b) wires of a dual-sensor probe in the same engine cycle (TAF procedure).

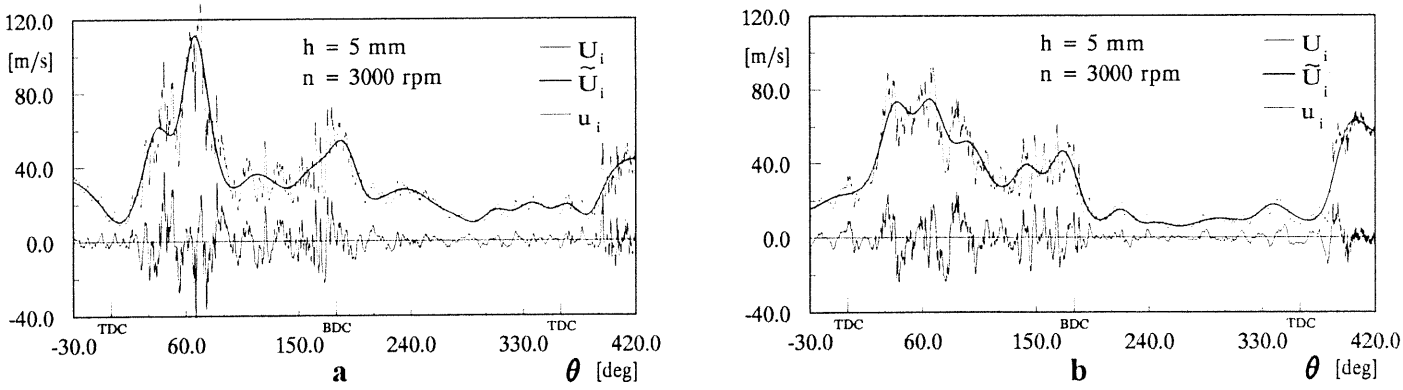


Fig. 8 - Instantaneous velocity, mean velocity and turbulent fluctuation obtained by single-sensor probes with axial (a) and tangential (b) wires in one engine cycle (TAF procedure).

velocity fluctuation $u_{i,E}$ of Fig. 6 larger structures are apparent than in the cycle-resolved turbulence $u_i$ of Fig. 7 derived from the same data. These can be related to the lower frequency cyclic variations in the mean flow [2]. A significant squish effect on the velocity fluctuations is evident from Figs. 6, 7 and 8 at the end of the compression and during the expansion strokes. It consists of an increase in both turbulence intensity and frequency content, particularly during the reverse-squish-flow phase after TDC.

Figure 9 compares the distributions of the ensemble-averaged mean velocity $U$ obtained by radial and tangential wires of single- and dual-sensor probes at the locations indicated, for the engine speed $n = 1500$ rpm. The good agreement between the results from both types of probe, which is well within the experimental uncertainties, showed that the mutual wire interference may be virtually nil in dual-sensor probes and, at the same time, flow disturbances induced by single-sensor probes may be negligible. Nevertheless, higher differences, even though comparable to the experimental uncertainty, may be expected between the ensemble-averaged mean velocities measured by single- and dual-sensor probes, particularly in the induction and reverse-squish flows, where instabilities occurred.

Two phases of the inlet flow can be distinguished from Fig. 9a. The first peak of $U_R$, in the early part of induction ($\theta \approx 30 \div 60$ deg), corresponds to a secondary jet formed at smaller valve lifts; the subsequent peak, occurring when the valve is completely open [1], is due to the main induction flow. The secondary jet is primarily controlled by the passage between the valve and its seat, as well as by the pressure drop through the valve, while the main flow is influenced by the port geometry, cylinder wall and piston movement. The sloped edge of the valve head seems to deflect the secondary jet downwards, as suggested by the decreasing of the first peak intensity at locations closer to the cylinder head (Fig. 9c). On the other hand, the second peak is more pronounced at $h = 5$ mm (Fig. 9a) and $h = 2$ mm (Fig. 9c) than at $h = 9$ mm (Fig. 9d), owing to the inlet port shape as well as to the valve lift effect on the main flow.

Figure 10 shows the ensemble-averaged mean cooling

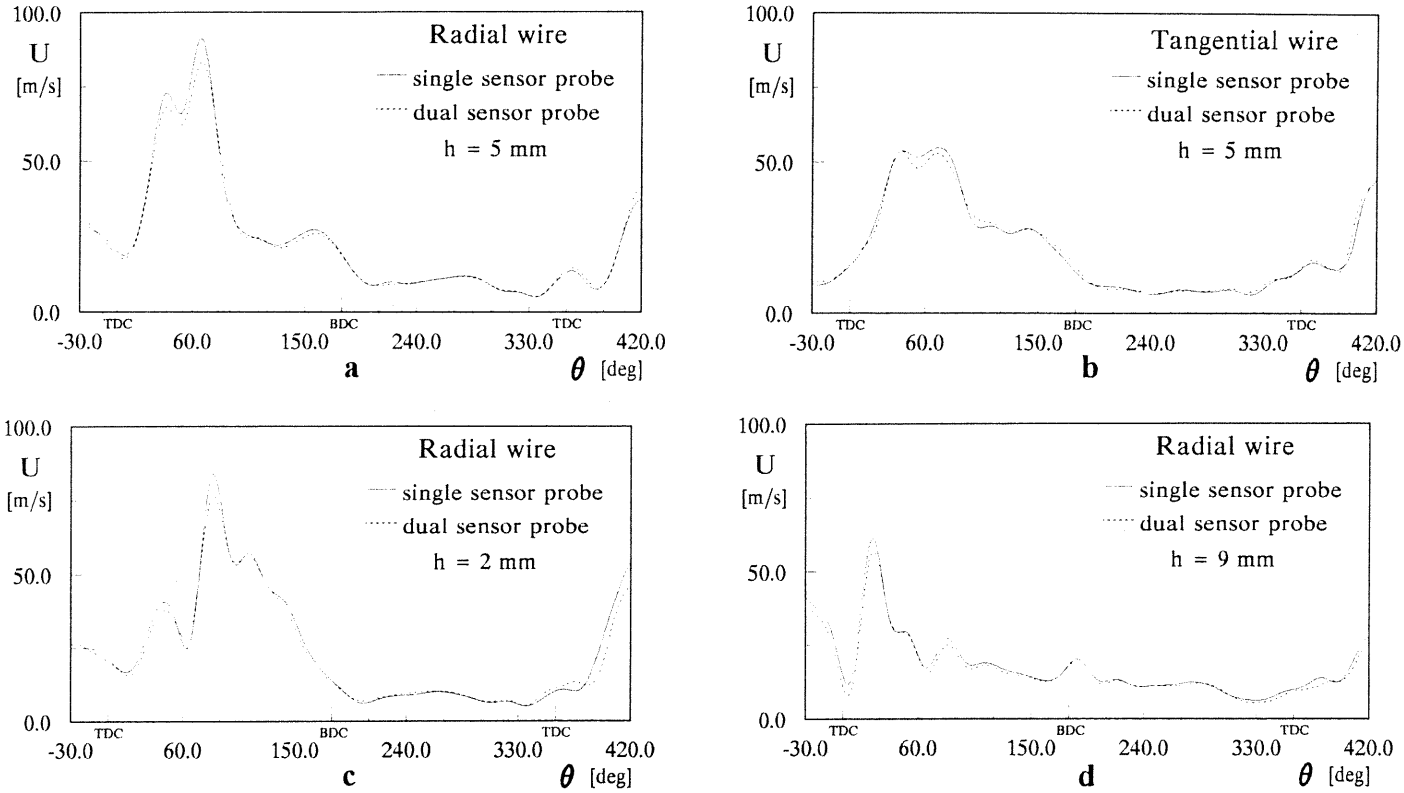


Fig. 9 - Ensemble-averaged mean velocity obtained by single- and dual-sensor probes at different locations along the injector axis (engine speed: 1500 rpm).

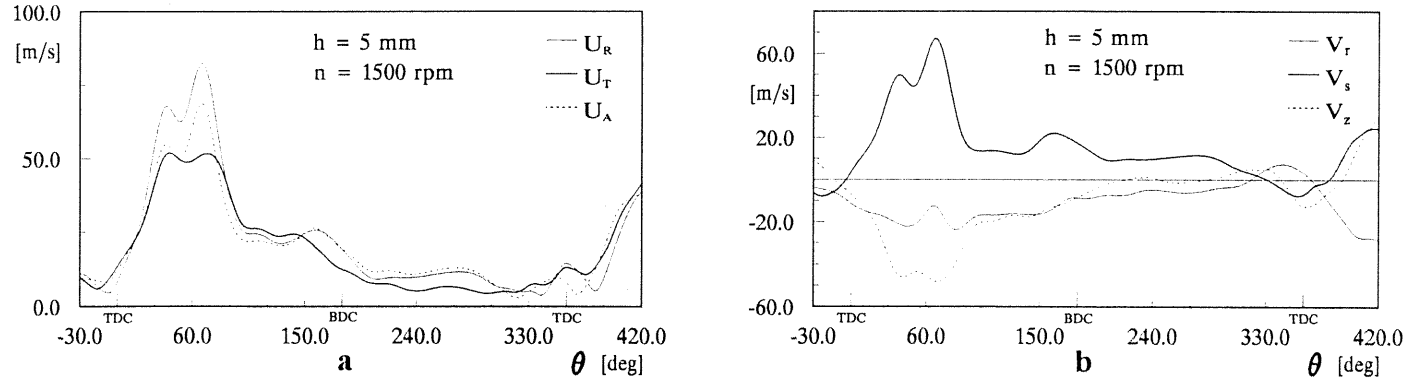


Fig. 10 - Distributions of ensemble-averaged mean cooling velocity (a) and related actual velocity components (b).

velocities $U_R$, $U_T$ and $U_A$ versus crank angle and the corresponding actual velocity components $V_r$, $V_s$ and $V_z$, obtained at a measuring point downstream to the valve and very close to the bowl axis ($h$ = 5 mm), and at $n$ = 1500 rpm. In Fig. 10b, the tangential and axial velocity patterns during the induction stroke are consistent with the trend of the bulk flow to spiral downwards like a counterclockwise helix. According to the above mentioned characteristics of the inlet flow, these velocity components show two peaks during the first half of the intake stroke: one at the early stage of inlet valve opening and the latter when the valve is completely open. It is also evident from Fig. 10b that the tangential (or swirl) component changes in direction at the end of the compression stroke, during the direct-squish phase; this change may suggest that, as the piston approaches the cylinder head, the bulk flow is forced into the bowl and the swirl center moves from the duct side to the opposite side with respect to the bowl axis, in agreement with the positive value of the radial velocity. During the reverse-squish phase the bulk flow leaves the bowl and moves back to the duct side, which conforms with the asymmetrical position of the bowl in the piston. Therefore, both the tangential and radial components change in direction. The axial velocity in Fig. 10b is directed downwards during induction, where it reaches the highest values. It is very low during compression, as expected, owing to the probe location close to the cylinder head. The fluctuations of $V_z$ may be ascribed to the flow pattern itself, as well as to the experimental uncertainties in cooling velocities, amplified in $V_z$ because of the low values of this component on compression. A downward axial--velocity increase is detected during the direct-squish phase, while a more relevant positive value of this component seems to occurr at the beginning of the expansion stroke.

Figure 11 plots, for a radial single-wire probe, the distributions of the turbulence intensity $u'$ (Figs. 11a,c) and of the cycle-resolved mean-velocity rms fluctuation $U_{rms}$

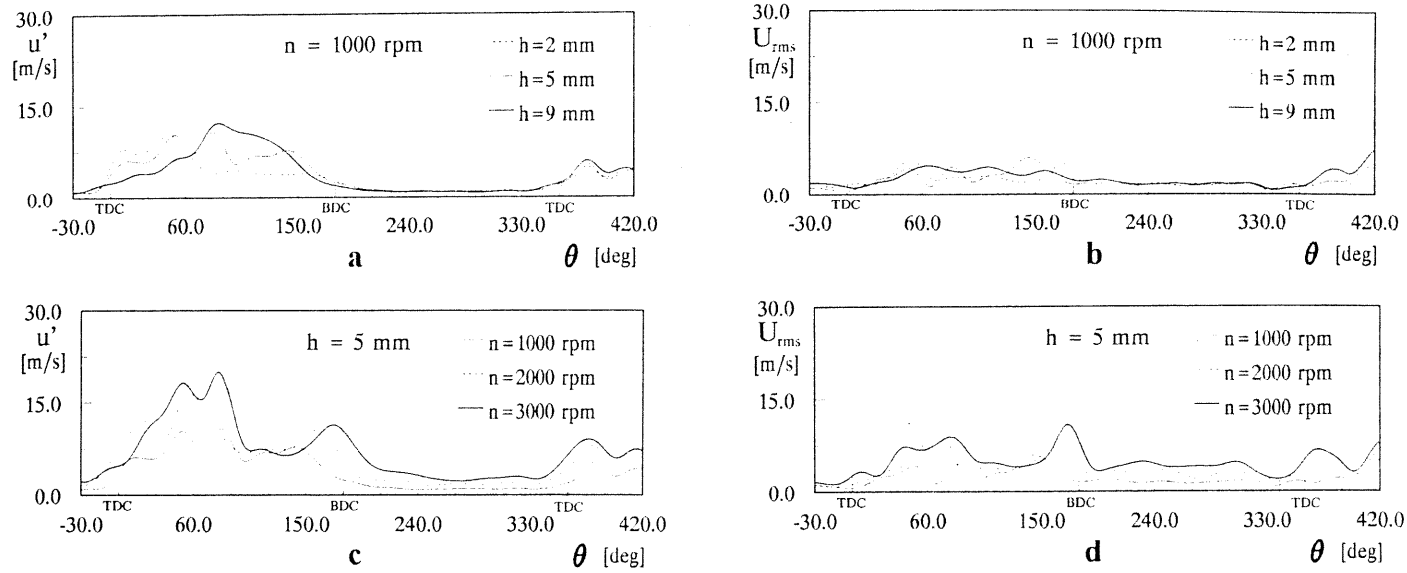


Fig. 11 - Turbulence intensity ($u'$) and in-cycle mean velocity rms fluctuation ($U_{rms}$) obtained by radial single-wire probe at different locations (a,b) (n=1000 rpm) and engine speeds (c,d) (h=5 mm).

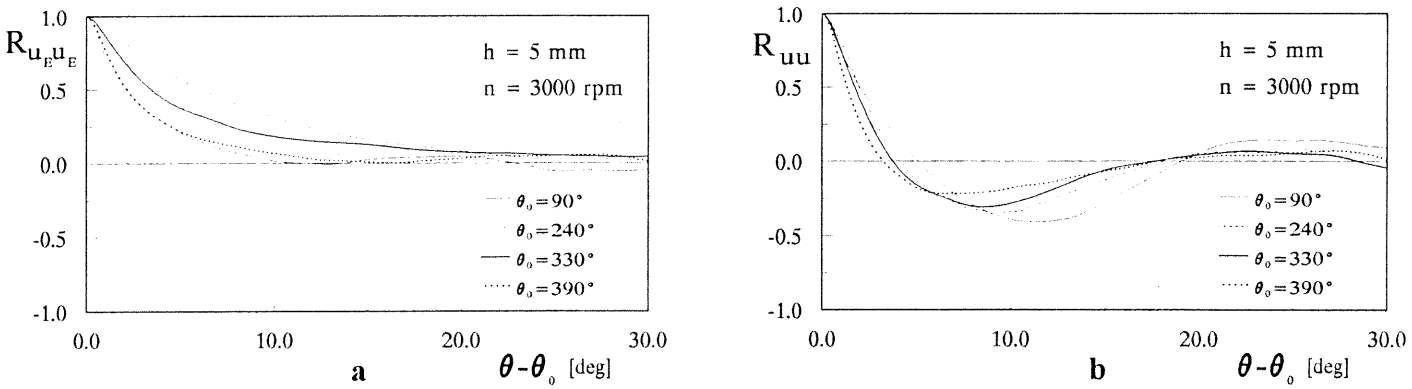


Fig. 12 - Autocorrelation coefficient of instantaneous (a) and cycle-resolved (b) velocity fluctuations obtained by single-sensor probe with radial wire at correlation intervals centered at different crank-angles $\theta_0$.

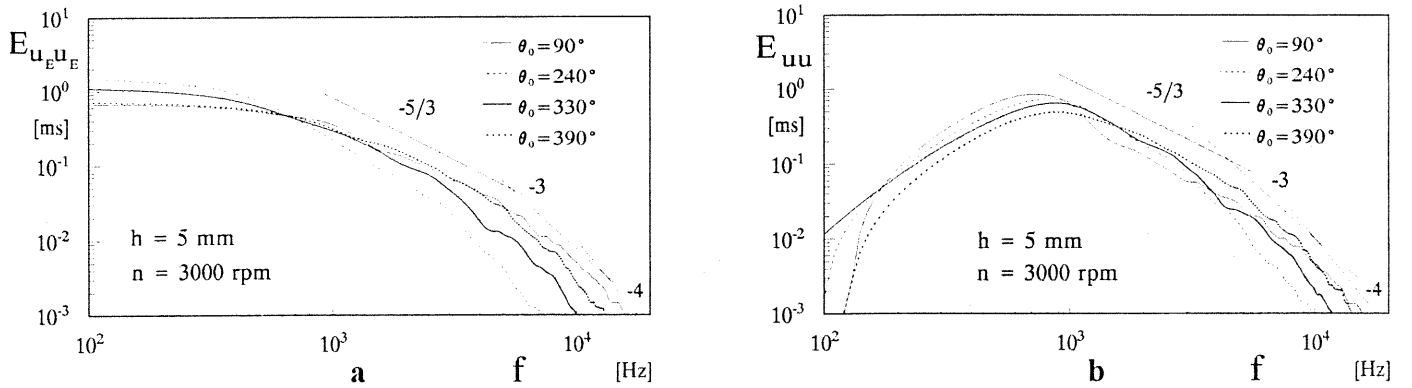


Fig. 13 - Autospectral density coefficient of instantaneous (a) and cycle-resolved (b) velocity fluctuations obtained by single-sensor probe with radial wire at correlation intervals centered at different crank-angles $\theta_0$.

(Figs. 11b,d) so as to give information about their dependence on measurement location (Figs. 11a,b) and engine speed (Figs. 11c,d). Both $u'$ and $U_{rms}$ are mainly sensitive to this latter showing an ordered trend to increase with it on the compression and the early expansion stroke (Figs. 11c,d). A less orderly increasing tendency with the engine speed can be observed on induction, reflecting the complexity of the flow.

The dependence of both $u'$ and $U_{rms}$ on the measurement location is negligible during the compression stroke (Figs. 11a,b). However (Fig. 11a), on early induction, higher turbulence intensities are detected close to the cylinder head ($h$ = 2 mm), while, on late induction, when the inlet valve is completely open, $u'$ increases farther from the head ($h$ = 9 mm). This can be explained by the fact that in both cases the measurement location was in the highly turbulent recirculating regions at the boundaries of the jet and main flow, respectively. At $h$ = 5 mm, $u'$ shows influences of both inlet flows. The rms fluctuation of the in-cycle mean velocity

(Fig. 11b) is almost independent of the measurement location during the induction and the compression stroke, while the reverse squish seems to further increase $U_{rms}$, the farther the locations are from the cylinder head.

The autocorrelation coefficients of the instantaneous velocity fluctuation and of the cycle-resolved turbulent fluctuation, obtained by single-sensor probe with radial wire, are reported in Fig. 12 versus the crank-angle separation interval $\theta - \theta_0$ (corresponding to time separation $\tau$ in equation (10)) for correlation intervals $\Phi$ of 60 deg, centered on the crank angles $\theta_0$ indicated. Fig. 13 shows the auto-spectral density coefficients obtained by applying equation (10) to the autocorrelation coefficients of Fig. 12. In Fig. 13 logarithmic scales are used to give emphasis to the high frequency range. The slopes -5/3, -3 and -4 are also marked in this figure, for analogy with wave number spectra [2, 11]. In the intermediate frequency range ($f \approx 1 \div 4$ kHz) the slope -5/3 could be approached by both cycle-resolved and instantaneous velocity fluctuation autospectra. As detailed elsewhere [2], the difference in the autocorrelation coefficients of the instantaneous (Fig. 12a) and cycle--resolved (Fig. 12b) velocity fluctuations is basically due to the autocorrelation of the low-frequency mean-velocity cyclic variations. From the decaying patterns of $R_{u_E u_E}$ and the autospectra frequency distributions, similar turbulence spectral structures can be recognized in the intake flow ($\theta_0 = 90$ deg) and in the reverse squish ($\theta_0 = 390$ deg), both having jet-flow features with a high frequency content. Based also on the results of Fig. 11, the reverse-squish flow can be considered to be a source of higher frequency and more intense turbulence than that produced by the direct squish ($\theta_0 = 330$ deg). This effect can be useful at the later combustion stages, for example, in order to enhance the mixing of soot-particle-laden regions with the excess air and their burn up.

## CONCLUSIONS

An advanced HWA technique using homemade probes with specifically oriented single and multiple wires has been applied to the analysis of the air mean- and fluctuating--motion in the combustion chamber of an automotive engine with a high squish in-piston bowl and one helicoidal intake duct. For the first time in-cylinder velocity measurements have been performed with dual-sensor probes which were assessed to bear virtually nil mutual wire interference and flow perturbation.

The three-dimensional mean-flow velocity components were resolved through the induction, compression and the early part of the expansion strokes, using shielded probes to remove any problems of directional ambiguity.

The intensity of turbulence and cycle-resolved mean--velocity fluctuation, was preliminarily investigated at several distances from the cylinder head, along the injector axis, and at different engine speeds, up to 3000 rpm. At this high speed, an insight was also given into the temporal evolution of the turbulence time-frequency structure along the engine cycle. The fluctuating motion, including the mean-flow cyclic variation, was shown to be more sensitive to the engine speed than to the measurement location and to increase less than proportionally with the former. The intensity and frequency content of the turbulence produced during the induction stroke, by both secondary jet and main swirling flows as well as by their interference, decayed on compression, while in the last part of this stroke, when the direct squish-flow occurred and in the reverse squish-flow phase during the expansion, an increase of both turbulence intensity and frequency was produced. It was found that the effects of the reverse squish as a source of high-frequency turbulent fine structures were more relevant than those of the direct squish, with features close to the intake flows.

## ACKNOWLEDGMENTS

This work was financially supported by C.N.R.-P.F.T. 2 (Consiglio Nazionale delle Ricerche - Progetto Finalizzato Trasporti 2) under Contract No. 92.01869.PF74.

## REFERENCES

1. Catania, A.E., Dongiovanni, C., Mittica, A., Molina, G., Morero, L., and Spessa, E., "A New Test Bench for HWA Fluid-Dynamic Characterization of a Two-Valved In--Piston-Bowl Production Engine," submitted to *SAE International Congress & Exposition*, Detroit, MI, 1995.
2. Catania, A.E., Dongiovanni, C., and Mittica, A., "Time-Frequency Spectral Structure of Turbulence in an Automotive Engine," *SAE Trans., Journal of Engines*, Vol. 101, Paper No. 920153, pp. 221-244, 1992.
3. Catania, A.E., "Induction System Effects on the Fluid-Dynamics of a D.I. Automotive Diesel Engine," *ASME Diesel & Gas Engines Symposium, ETCE*, Paper No. 85-DGP-11, 1985.
4. Catania, A.E., and Mittica, A., "Induction System Effects on Small-Scale Turbulence in a High-Speed Diesel Engine," *ASME Trans., Journal of Engineering for Gas Turbines and Power*, Vol. 109, pp. 491-502, 1987.
5. Witze, P.O., "A Critical Comparison of Hot-Wire Anemometry and Laser Doppler Velocimetry for I.C. Engine Applications," *SAE Trans.*, Vol. 89, Paper No. 800132, pp. 711-739, 1980.
6. Catania, A.E., and Mittica, A., "Extraction Techniques and Analysis of Turbulence Quantities from In-Cylinder Velocity Data," *ASME Trans., Journal of Engineering for Gas Turbines and Power*, Vol. 111, pp. 466-478, 1989.
7. Catania, A.E., and Mittica, A., "Autocorrelation and Autospectra Estimation of Reciprocating Engine Turbulence," *ASME Trans., Journal of Engineering for Gas Turbines and Power*, Vol. 112, pp. 357-368, 1990.
8. Catania, A.E., Dongiovanni, C., and Mittica, A., "Further Investigation into the Statistical Properties of Reciprocating Engine Turbulence," *JSME International Journal*, Series II, Vol. 35, No. 2, pp. 255-265, 1992.
9. Hinze, J.O., *Turbulence*, Mc Graw-Hill, New York, 1975.
10. Bendat, J.S., and Piersol, A.G., *Random Data: Analysis and Measurement Procedures*, 2nd Ed., John Wiley & Sons, New York, 1986.
11. Lesieur, M., *Turbulence in Fluids*, Martinus Nijhoff Publishers, Dordrecht, 1987.